View metadata, citation and similar papers at core.ac.uk

brought to you by CORE

provided by Sydney eScholarship

Solar Physics
DOI: 10.1007/•••••-•••-•••-••••-•

A Check on the Validity of Magnetic Field Reconstructions

A. Mastrano[1] · M. S. Wheatland[1] · S. A. Gilchrist[2]

© Springer ••••

Abstract We investigate a method to test whether a numerically computed model coronal magnetic field $\boldsymbol{B}$ departs from the divergence-free condition (also known as the solenoidality condition). The test requires a potential field $\boldsymbol{B}_0$ to be calculated, subject to Neumann boundary conditions, given by the normal components of the model field $\boldsymbol{B}$ at the boundaries. The free energy of the model field may be calculated using $\frac{1}{2\mu_0}\int(\boldsymbol{B}-\boldsymbol{B}_0)^2\mathrm{d}V$, where the integral is over the computational volume of the model field. A second estimate of the free energy is provided by calculating $\frac{1}{2\mu_0}\int \boldsymbol{B}^2\,\mathrm{d}V - \frac{1}{2\mu_0}\int \boldsymbol{B}_0^2\,\mathrm{d}V$. If $\boldsymbol{B}$ is divergence-free, the two estimates of the free energy should be the same. A difference between the two estimates indicates a departure from $\nabla\cdot\boldsymbol{B}=0$ in the volume. The test is an implementation of a procedure proposed by Moraitis *et al.* (*Sol. Phys.* **289**, 4453, 2014) and is a simpler version of the Helmholtz decomposition procedure presented by Valori *et al.* (*Astron. Astrophys.* **553**, A38, 2013). We demonstrate the test in application to previously published nonlinear force-free model fields, and also investigate the influence on the results of the test of a departure from flux balance over the boundaries of the model field. Our results underline the fact that, to make meaningful statements about magnetic free energy in the corona, it is necessary to have model magnetic fields which satisfy the divergence-free condition to a good approximation.

Keywords: Active Regions, Magnetic Fields; Magnetic Fields, Corona; Magnetic Fields, Models

✉ A. Mastrano
alpha.mastrano@sydney.edu.au

M. S. Wheatland
michael.wheatland@sydney.edu.au

S. A. Gilchrist
sgilchrist@nwra.com

[1] Sydney Institute for Astronomy, School of Physics, University of Sydney, NSW 2006, Australia

[2] NorthWest Research Associates, Boulder, CO 80301-2245, USA

1. Introduction

Accurate knowledge of coronal magnetic field structure is important for understanding the physics and energetics of solar flares. Knowledge of magnetic free energy (the energy of the non-potential field component of the magnetic field) may be useful for predicting solar flares (Barnes *et al.*, 2016). The coronal magnetic field, unfortunately, cannot be measured directly. A popular approach to modelling the coronal field is the nonlinear force-free field (NLFFF) reconstruction. In this approach, the coronal field $\boldsymbol{B}$ is assumed to be force-free *i.e.* the Lorentz force, $(\nabla \times \boldsymbol{B}) \times \boldsymbol{B}$, vanishes. The nonlinear force-free equations are solved numerically using vector magnetogram data as the boundary conditions. The equations to be solved are:

$$\nabla \times \boldsymbol{B} = \alpha \boldsymbol{B}, \tag{1}$$

where α is the force-free parameter, together with the divergence-free condition[1]

$$\nabla \cdot \boldsymbol{B} = 0. \tag{2}$$

There are many possible methods to solve the NLFFF equations. DeRosa *et al.* (2015) compared the results of five codes, using three different methods (optimization, magnetofrictional, and Grad-Rubin), in reconstructing the coronal field of Active Region (AR) 10978 on 13 December 2007. The codes differ in their methods of solution of Equations 1 and 2, and also in how they treat the vector magnetogram data. Accurate numerical solutions to the NLFFF equations should satisfy the divergence-free condition, but inconsistency between boundary data and the model can lead to departures from this condition. Also, the models are constructed on a discrete grid, and truncation error (discretisation error) in the numerical evaluation of the derivatives gives non-zero values of $\nabla \cdot \boldsymbol{B}$. Valori *et al.* (2013) presented a method for testing departures of NLFFF solutions from $\nabla \cdot \boldsymbol{B} = 0$ based on Thomson's theorem. In this method, the field is decomposed into a potential component $\boldsymbol{B}_0$ and a current-carrying component $\boldsymbol{B}_\mathrm{c}$, which are then further decomposed into solenoidal and non-solenoidal components. The energies of the components are then compared (Valori *et al.*, 2013; DeRosa *et al.*, 2015). Ideally, the energies of the non-solenoidal components, which are unphysical, should vanish, but in practice, these energies are non-zero. DeRosa *et al.* (2015) showed that in the worst cases, the unphysical contributions to the energy may be as large as the free energy of the field, *i.e.* the energy of the solenoidal component of $\boldsymbol{B}_\mathrm{c}$.

Although the Valori *et al.* (2013) method is an informative test of the reliability of NLFFF reconstructions, it has not been much used. That is likely because it requires Helmholtz decomposition of the fields $\boldsymbol{B}_0$ and $\boldsymbol{B}_\mathrm{c}$, which is a non-trivial procedure.

In this article, we investigate a simple test on the validity of NLFFF models. This test is a re-implementation of a procedure used by Moraitis *et al.* (2014)

[1]Also known as the solenoidality condition.

to benchmark their method of calculating free energy and magnetic helicity. Su *et al.* (2014) and Moraitis *et al.* (2016) later used the test to gauge the accuracy of energy calculations of solar active regions. The test compares the magnetic free energy obtained directly from volume-integrating the square of the current-carrying (*i.e.* non-potential) field component and that obtained by subtracting the energy of the potential field from the total magnetic field energy. If the total field divergence vanishes (as it ideally should), the two methods of calculating free energy give the same result. The version of this test that we present here is conceptually similar to the method of Valori *et al.* (2013), but is much simpler to apply.

The article is structured as follows. In Section 2, we describe the two different methods of calculating free energy and show how they give the same result if the field is divergence-free. In Section 3, we apply our test to a published set of results from different NLFFF codes, the same data analyzed by DeRosa *et al.* (2015). In Section 4 we discuss the effects of flux-imbalanced boundaries on our calculations. In Section 5, we summarize our results.

2. Method

Consider a given magnetic field $\boldsymbol{B}$. Following Moraitis *et al.* (2014), we decompose the field $\boldsymbol{B}$ into a potential component $\boldsymbol{B}_0$ and a current-carrying component $\boldsymbol{B}_\mathrm{c}$:

$$\boldsymbol{B} = \boldsymbol{B}_0 + \boldsymbol{B}_\mathrm{c}. \tag{3}$$

We construct

$$\boldsymbol{B}_0 = \nabla\phi \tag{4}$$

from $\boldsymbol{B}$ by solving

$$\nabla^2\phi = 0, \tag{5}$$

subject to the Neumann boundary condition

$$\hat{\boldsymbol{n}} \cdot \nabla\phi = \hat{\boldsymbol{n}} \cdot \boldsymbol{B}_0 = \hat{\boldsymbol{n}} \cdot \boldsymbol{B} \tag{6}$$

on the boundary surface S. The total magnetic field energy is

$$W_B = \frac{1}{2\mu_0} \int \boldsymbol{B}^2 \, \mathrm{d}V, \tag{7}$$

and the energy of the potential field is

$$W_0 = \frac{1}{2\mu_0} \int \boldsymbol{B}_0^2 \, \mathrm{d}V. \tag{8}$$

The magnetic free energy W_f1 is the energy of the field $\boldsymbol{B}_\mathrm{c}$:

$$W_\mathrm{f1} = \frac{1}{2\mu_0} \int \boldsymbol{B}_\mathrm{c}^2 \, \mathrm{d}V = \frac{1}{2\mu_0} \int (\boldsymbol{B} - \boldsymbol{B}_0)^2 \, \mathrm{d}V. \tag{9}$$

Using Equations 3 and 4, we can show that

$$W_{\rm f1} = W_B - W_0 - \frac{1}{\mu_0}\int_{\partial V} \phi \boldsymbol{B}_{\rm c} \cdot {\rm d}\boldsymbol{S} + \frac{1}{\mu_0}\int \phi \nabla \cdot \boldsymbol{B}_{\rm c}\ {\rm d}V, \tag{10}$$

where ${\rm d}\boldsymbol{S} = \hat{\boldsymbol{n}}{\rm d}S$ and ${\rm d}S$ is the infinitesimal area element on S. The third term on the right-hand side of Equation 10 vanishes because

$$\hat{\boldsymbol{n}} \cdot \boldsymbol{B}_{\rm c} = 0 \tag{11}$$

on S. The integrand in the last term can be written as $\phi \nabla \cdot \boldsymbol{B}$, assuming an accurate solution to Equation 5 (Laplace's equation) has been obtained, so that $\nabla \cdot \boldsymbol{B}_0 = 0$. Therefore, we have

$$W_{\rm f1} = W_{\rm f2} + \frac{1}{\mu_0}\int \phi \nabla \cdot \boldsymbol{B}\ {\rm d}V, \tag{12}$$

with

$$W_{\rm f2} = W_B - W_0. \tag{13}$$

Equation 12 tells us that, if $\nabla \cdot \boldsymbol{B} = 0$ in the volume, then the free energy

$$W_{\rm f1} = \frac{1}{2\mu_0}\int (\boldsymbol{B} - \boldsymbol{B}_0)^2\ {\rm d}V \tag{14}$$

is the same as

$$W_{\rm f2} = \frac{1}{2\mu_0}\int \boldsymbol{B}^2\ {\rm d}V - \frac{1}{2\mu_0}\int \boldsymbol{B}_0^2\ {\rm d}V. \tag{15}$$

If the divergence is non-zero, then these two "free energies" may differ. Thus, to check whether a model field is divergence-free or not, one simply compares $W_{\rm f2}$ to $W_{\rm f1}$. Note, however, that $W_{\rm f1} = W_{\rm f2}$ is a necessary but not sufficient condition for a divergence-free field. If $\nabla \cdot \boldsymbol{B} = 0$, then $W_{\rm f1} = W_{\rm f2}$, but $W_{\rm f1} = W_{\rm f2}$ does not necessarily imply that $\nabla \cdot \boldsymbol{B} = 0$.

The first step in our method is the construction of the potential field. To do this, we use the Checkerboard Relaxation Method Used for Potential field reconstruction (CRUMP) code. CRUMP solves Laplace's equation for the scalar potential ϕ in a Cartesian domain with Neumann boundary conditions (defined by the normal components of $\boldsymbol{B}$ at the six boundary surfaces), using a successive over-relaxation scheme with checkerboard updating (Press *et al.*, 1992).[2] We note that, in principle, the $\boldsymbol{B}_0$ component can be calculated using any method, as long as the end result satisfies the conditions given by Equations 3–6.

After $\boldsymbol{B}_0$ has been calculated, we calculate W_B, W_0, $W_{\rm f1}$ and $W_{\rm f2}$, defined by Equations 7, 8, 9, and 13. We use the trapezoidal method [see *e.g.* Press

[2]Further details of the CRUMP code are discussed in the Appendix.

et al. (1992)] to perform the volume integrals. To compare the two free-energy estimates, we calculate the fractional difference

$$\varepsilon = \left| \frac{W_{\rm f2} - W_{\rm f1}}{W_{\rm f2}} \right| . \tag{16}$$

This quantity is similar to the relative energy error r defined by Su *et al.* (2014) and Moraitis *et al.* (2016).

In Section 3, we apply this test to the results obtained with five different NLFFF codes in modelling the coronal magnetic field of AR 10978 on 13 December 2007.

3. Application

In this section, we apply our divergence-free test to the five NLFFF codes previously compared and analyzed by DeRosa *et al.* (2015).

3.1. A Summary of the NLFFF Codes

The five codes that we examine, using the test described in Section 2, implement three different methods of solving the NLFFF equations (on a uniform, three-dimensional Cartesian grid with equal spacing in all dimensions), namely the optimization, magnetofrictional, and three Grad-Rubin methods. The codes and methods are as follows (DeRosa *et al.*, 2015)[3].

i) Optimization, which uses a relaxation scheme that seeks to minimize a volume integral combining the Lorentz force and the divergence of $\boldsymbol{B}$. If this volume integral is successfully reduced to zero, the field is guaranteed to be force-free and divergence-free (Wheatland, Sturrock, and Roumeliotis, 2000; Wiegelmann and Inhester, 2010; Wiegelmann *et al.*, 2012). The optimization method involves evolution of a field $\boldsymbol{B}$ which explicitly departs from $\nabla \cdot \boldsymbol{B} = 0$ at intermediate evolution times.

ii) Magnetofrictional, which advances the magnetic field in time through the magnetic induction equation, with the velocity field given by the momentum equation (Valori, Kliem, and Fuhrmann, 2007; Valori *et al.*, 2010).

iii) Grad-Rubin, which solves for and updates $\boldsymbol{B}$ and the force-free parameter α iteratively, using the normal component of the field at the boundary and the value of the force-free parameter α over one polarity of the field as boundary conditions. Grad-Rubin codes may obtain different results depending on which polarity is chosen for the boundary conditions on α. We include both the P solutions (where α values are taken from the positive magnetic

[3]The solution volumes are available for download from http://dx.doi.org/10.7910/DVN/7ZGD9P.

polarity points) and N solutions (where α values are taken from points of negative magnetic polarity) of the Grad-Rubin codes in our comparison below. The Grad-Rubin method is implemented by three different codes analyzed in this article:

- CFIT, which works with a vector potential $\boldsymbol{B} = \nabla \times \boldsymbol{A}$ (and so should preserve $\nabla \cdot \boldsymbol{B} = 0$ to truncation, *i.e.* discretisation error). The method iteratively solves the Poisson equation by a two-dimensional Fourier method using currents in the volume obtained by field line tracing of values of α at each iteration. If the iterations achieve a fixed point, the result is force-free [see Wheatland (2007) for full details],
- XTRAPOL, which solves a mixed boundary value problem for α and $\boldsymbol{B}$ using a finite-difference approach on the vector potential $\boldsymbol{A}$ on a staggered mesh, ensuring $\nabla \cdot \boldsymbol{B} = 0$ to rounding errors [see Amari, Boulmezaoud, and Aly (2006) for full details], and
- FEMQ, which solves the same boundary value problem as XTRAPOL using a finite-element approach directly on $\boldsymbol{B}$, minimizing $\nabla \cdot \boldsymbol{B}$ by a least-squares approach [see Amari, Boulmezaoud, and Aly (2006) for full details].

3.2. Results of the Divergence-free Test

DeRosa *et al.* (2015) presented the results of applying the five codes to vector magnetograms constructed from *Hinode Solar Optical Telescope Spectro-Polarimeter* data for AR 10978 on 13 December 2007. The magnetograms were constructed for different spatial resolutions by rebinning the spectral data by factors 2, 3, 4, 6, 8, 10, 12, 14, and 16. The data are referred to by the bin size, *e.g.* bin 2 is the highest resolution magnetogram, involving rebinning by a factor of 2. The actual sizes of the original and binned data are summarized in Table 1 of DeRosa *et al.* (2015).[4]

We apply the divergence-free test described in Section 2 to each NLFFF solution data cube. Figure 1 shows the fractional difference ε between the two free energies as a function of bin size for each NLFFF solution. For the Grad-Rubin codes (CFIT, XTRAPOL, and FEMQ), we show both the P and N solutions. The results broadly agree with those of DeRosa *et al.* (2015). In general, we find that $W_{\rm f2} > W_{\rm f1}$, but the two energies are comparable, except for the optimization code, where $W_{\rm f2} \approx 2W_{\rm f1}$. This corresponds to the observation of DeRosa *et al.* (2015), that, in the optimization solutions, the magnitudes of the energies of the mixed non-solenoidal component are of the same order as the free energy. Like DeRosa *et al.* (2015), we find that, except for optimization, the results for the larger bin-size (*i.e.* lower spatial resolution) calculations generally depart further from the divergence-free condition. The results for the optimization code seem

[4]To make a meaningful comparison between the models, the analysis volume is chosen to be the largest common volume for all codes and resolutions. The volume does not include the entire available AR 10978 data.

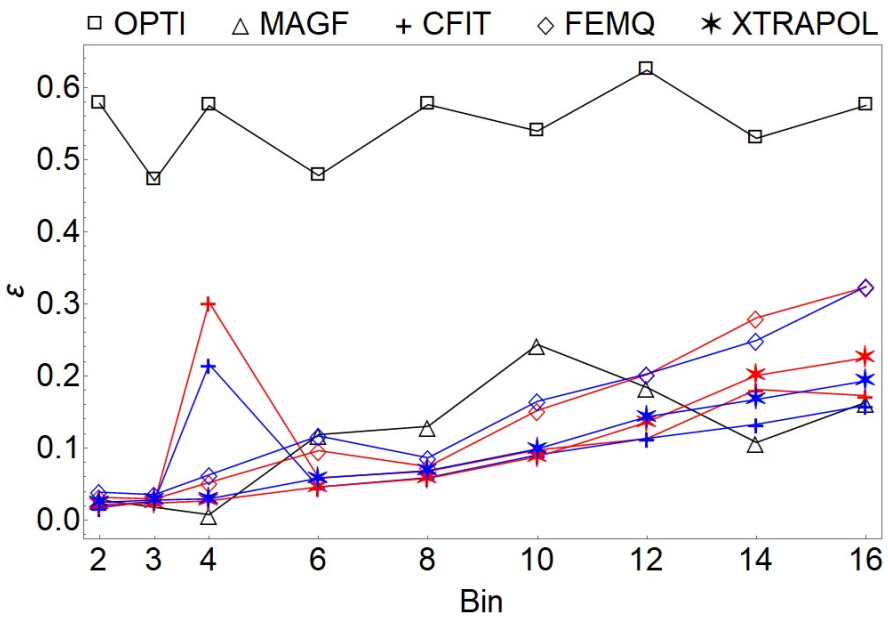

Figure 1. Comparison of the fractional difference between $W_{\rm f1}$ and $W_{\rm f2}$, expressed as $\varepsilon = |(W_{\rm f2} - W_{\rm f1})/W_{\rm f2}|$, for the five different codes [optimization (OPTI), magnetofrictional (MAGF), and the three Grad-Rubin codes CFIT, XTRAPOL, FEMQ] at different bin sizes. For the three Grad-Rubin codes (CFIT, XTRAPOL, FEMQ), we show the results of the P (blue solid curves) and N (red dashed curves) calculations, where the values of α are taken from points of positive magnetic polarity and negative magnetic polarity, respectively.

largely independent of bin size: the values of ε for the optimization method are the largest of the values for the five codes compared in this article, regardless of bin size.

The Grad-Rubin codes seem to follow the general trend that ε increases as bin size increases. We find that the CFIT solutions (both P and N) have a sudden jump in ε at bin 4, which does not follow this trend. The reason for this, as noted by DeRosa *et al.* (2015), is unknown. This particular solution from the code appears to be less accurate than the other solutions from CFIT. The other two Grad-Rubin codes (XTRAPOL and FEMQ) give solutions that follow the general trend closely (although FEMQ has higher ε at bin 6 than 8). XTRAPOL tends to have lower ε than FEMQ as bin size increases. At the highest and lowest resolutions we examine, CFIT (specifically, its P solution) has the lowest ε of the five codes.

The magnetofrictional code tracks the trend followed by the Grad-Rubin codes, although it has lower ε than all the other codes at bins 4 and 14, and higher ε than the others (except optimization) at bin 10. At bin 16, the ε of the magnetofrictional code is only slightly higher than that of CFIT (P solution).

In general, we conclude that the magnetofrictional and Grad-Rubin codes produce results consistent with $\nabla \cdot \boldsymbol{B} = 0$ to a comparable degree. The optimization code does not achieve $\nabla \cdot \boldsymbol{B} = 0$ to the same degree.

4. Flux Balance

It is important to recognise that, if the model magnetic field in the volume of interest has a net incoming or outgoing flux over the surfaces of the computational volume, it is not possible to generate a corresponding divergence-free potential field by solving Laplace's equation subject to Neumann boundary conditions, *e.g.* using CRUMP. The net flux is given by

$$\Phi_{\rm net} = \int \boldsymbol{B} \cdot {\rm d}\mathbf{S} = \int \boldsymbol{B}_0 \cdot {\rm d}\mathbf{S}, \tag{17}$$

so if $\boldsymbol{B}_0 = \nabla\phi$ then using Gauss's law we have

$$\int \nabla^2\phi \, {\rm d}V = \Phi_{\rm net}. \tag{18}$$

Equation 18 implies that if $\Phi_{\rm net} \neq 0$ it is not possible to satisfy $\nabla^2\phi = 0$ everywhere in the volume.

Hence it is also necessary to check for flux balance. In Figure 2 we compare the ratio of outgoing fluxes to unsigned fluxes over the surface of the computational volume, for each of the NLFFF model fields. All of the model fields analyzed here are flux-imbalanced to a very small degree, $\approx 1\%$. The integrand in the last term on the right-hand side of Equation 10 can be written $\phi\nabla\cdot(\boldsymbol{B}-\boldsymbol{B}_0)$. The departure from solenoidality can therefore be due to a contribution from a non-zero divergence of $\boldsymbol{B}_0$ as well as a non-zero divergence of $\boldsymbol{B}$. While our method cannot distinguish between the sources of non-solenoidality, comparison between the Helmholtz decompositions of the model fields shows that the mixed non-solenoidal component (containing contributions from both the potential field and the current-carrying field) is energetically important in a number of the solutions (DeRosa *et al.*, 2015).

Furthermore, for all the NLFFF reconstructions discussed here, DeRosa *et al.* (2015) found that the energy of the non-solenoidal part of the potential field is smaller than the energy of the solenoidal part of the potential field by at least three orders of magnitude. They also found that all the model fields have comparable non-solenoidal potential field energies, even the magnetofrictional field (whose bin 8 result has the largest flux imbalance, $\approx 2\%$). This indicates that flux imbalance of $\approx 1\%$ leads to negligible error in the field energies and that the relation between flux imbalance and non-solenoidality is not straightforward, *i.e.* flux imbalance does not necessarily lead to a proportional increase in the energy of the non-solenoidal part of the potential field or, consequently, ε.

We investigate the effect of flux imbalance on solenoidality further by applying the solenoidality test to an artificially constructed nonlinear force-free magnetic bipole field. The boundary field $B_z(x, y, z = 0)$ is constructed in the region $0 \leqslant x \leqslant 1$, $0 \leqslant y \leqslant 1$. In dimensionless units, B_z at the bottom boundary of the volume is

$$\begin{aligned} B_z(x, y, z = 0) = {} & B_{\rm max} \exp[-c_1(x - 0.5)^2 - c_1(y - 0.6)^2] \\ & - B_{\rm max} \exp[-c_2(x - 0.5)^2 - c_2(y - 0.4)^2], \end{aligned} \tag{19}$$

where we set $B_{\rm max}$ such that the maximum absolute field strength is 1, and $c_1 = c_2 = 50$. The boundary condition on the force-free parameter α is

$$\alpha(x, y, z = 0) = \begin{cases} 6, \text{ if } B_z(x, y, z = 0) \geqslant 0.8, \\ 0, \text{ otherwise,} \end{cases} \tag{20}$$

in dimensionless units.[5] The plot of $B_z(x, y, z = 0)$ is shown in Figure 3. We use the Grad-Rubin code CFIT (Wheatland, 2007) to calculate a NLFFF solution in the region $0 \leqslant x \leqslant 1$, $0 \leqslant y \leqslant 1$, $0 \leqslant z \leqslant 0.5$, with the calculation performed on a $200 \times 200 \times 100$ grid, then we use CRUMP to calculate a potential field satisfying Equation 6.

Flux imbalance is introduced by adding a background vertical field at $z = 0$, where $B_z(x, y, z = 0) < 0.01$. We consider a constant background field and a randomly-distributed field with a non-zero mean. Additionally, we enforce $B_z = 0$ at the top of the computational volume. The NLFFF solution calculated by CFIT is periodic in x and y, so that any unbalanced flux introduced at the bottom of the volume must exit through the top of the volume. Closing the top of the volume (*i.e.* enforcing $B_z = 0$ at the top) ensures that the solution is flux-imbalanced for our test purposes.

To check the solenoidality of the solutions, we plot ε as a function of flux imbalance in Figure 4. We find similar values of ε for the uniform background and the randomly-distributed background. We also find that a flux imbalance of $\approx 2\%$ (equal to that of the bin 8 result of the magnetofrictional code discussed in Section 3) indeed has no noticeable effect on ε. We find, however, that a flux imbalance of $\gtrsim 6\%$ potentially leads to a large effect on ε, *e.g.* $|\varepsilon| = 0.35$ for a 10% flux imbalance. Our results may be dependent on the method of construction of the nonlinear force-free field with flux-imbalanced boundaries. However, they suggest that, if one finds large ε, one needs to check the solution volume for flux imbalance before drawing conclusions on the solenoidality of the solution.

Figure 5 shows W_0 and W_B plotted *versus* the flux imbalance, with the energies normalized to the flux-balanced value. The changes in energy are very small: for the potential field energy (top panel) the maximum change is about 1%, whereas for the total field energy (bottom panel) the maximum change is about 0.07%. Figure 6 shows the free energy estimates $W_{\rm f1}$ and $W_{\rm f2}$ *versus* flux imbalance. The values of $W_{\rm f1}$ show an overall increase with flux imbalance (top panel), whereas $W_{\rm f2}$ decreases uniformly with flux imbalance (bottom panel).

Note that, strictly speaking, if there is a flux imbalance over the surface of the computational volume, then the reference field $\boldsymbol{B}_0$ is not a solution to Equation 5. In that case, the energy of $\boldsymbol{B}_0$ cannot be used as the reference energy to calculate the free energy of the field $\boldsymbol{B}$.

We have used as a reference potential field $\boldsymbol{B}_0$ the solution to Laplace's equation with Neumann boundary condition defined by the normal component of the field $\boldsymbol{B}$ on the boundaries of the computational domain. In practice other

[5]The parameter α must be non-zero, so that the final field configuration has non-zero $\boldsymbol{B}_{\rm c}$, $W_{\rm f1}$, and $W_{\rm f2}$.

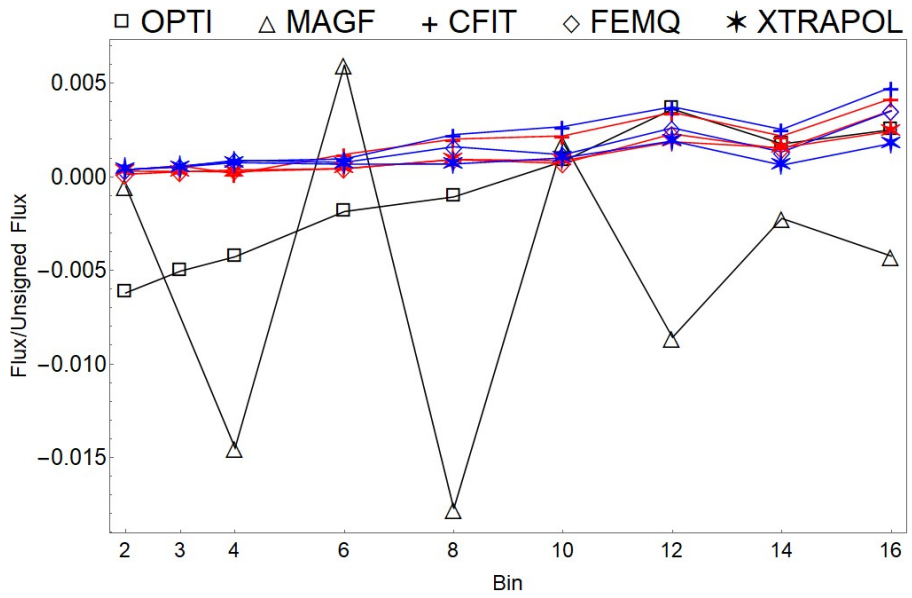

Figure 2. Ratio of the outgoing flux to unsigned flux over the surface of the computational volume for the model fields from the five different codes [optimization (OPTI), magnetofrictional (MAGF), and the three Grad-Rubin codes CFIT, XTRAPOL, FEMQ]. For the three Grad-Rubin codes (CFIT, XTRAPOL, FEMQ), we show the fluxes of the P (blue solid curves) and N (red dashed curves) calculations, where the values of α are taken from points of positive magnetic polarity and negative magnetic polarity, respectively.

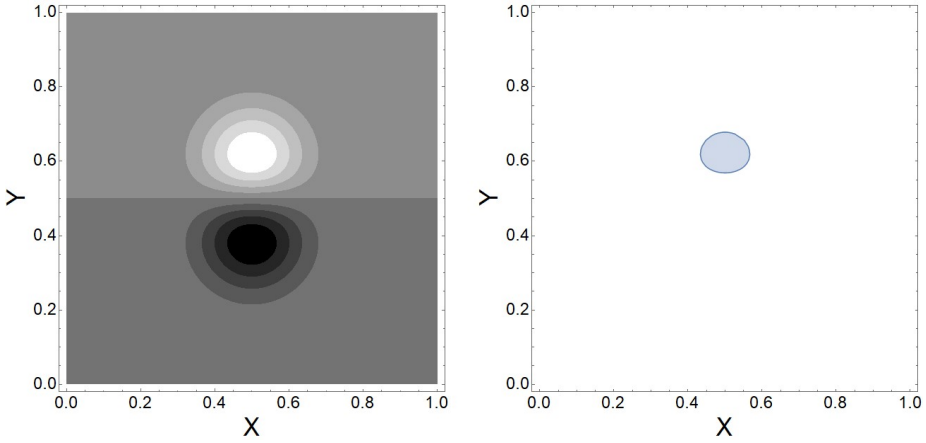

Figure 3. The boundary conditions for the vertical component of the magnetic field, $B_z(x, y, z = 0)$, and the force-free parameter, $\alpha(x, y, z = 0)$, for the bipole test case in the absence of flux imbalance. The left-hand panel shows a top-down view, with white (black) contours for positive (negative) B_z, the right-hand panel shows a top-down view of the region where $\alpha \neq 0$.

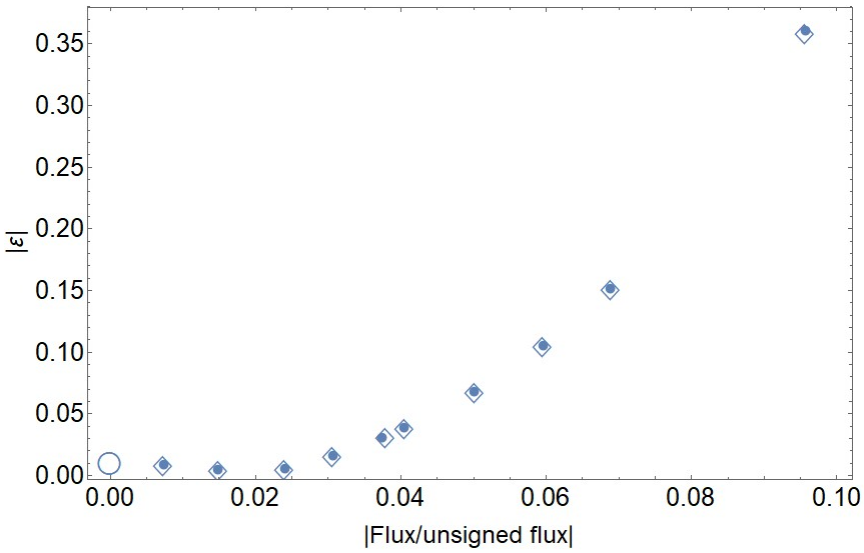

Figure 4. The fractional difference between W_{f1} and W_{f2}, expressed as $\varepsilon = |(W_{\mathrm{f2}} - W_{\mathrm{f1}})/W_{\mathrm{f2}}|$ as a function of the ratio of flux to unsigned flux for a bipole test case. The empty circle is the flux-balanced case, the filled circles are the uniform background case, and the diamonds are the random background case.

reference potential fields are also used by researchers modeling magnetic fields. For example, it is common to construct potential fields using just the boundary conditions on the lower boundary of the computational domain, using *e.g.* a Fourier (Alissandrakis, 1981), or a Green's function solution (Chiu and Hilton, 1977) to Laplace's equation. If the reference potential field does not satisfy Equation 6 on all boundaries, then the potential field does not satisfy Thomson's theorem, and does not represent the state with the minimum energy for a given distribution of magnetic field on the boundaries. In this case, the energy of the potential field cannot be used as a physically meaningful reference energy for calculating the free energy of the field.

5. Conclusions

In this article, we re-implement a test proposed by Moraitis *et al.* (2014) to check whether a constructed NLFFF model field $\boldsymbol{B}$ is divergence-free or not. We applied the test to the results for the five codes analyzed by DeRosa *et al.* (2015) and our conclusions on the solenoidality of the results of the codes and the effects of spatial resolution agree with the results obtained in that paper using the method of Valori *et al.* (2013). Unlike the Valori *et al.* (2013) procedure, the test does not require a Helmholtz decomposition of $\boldsymbol{B}$ and analysis of the energies of the different components of a field. This test requires only the calculation of the potential field component, subject to Neumann boundary conditions, given by the normal components of $\boldsymbol{B}$ at the boundaries. Then we simply compare $W_{\mathrm{f1}} = (1/2\mu_0)\int(\boldsymbol{B}^2 - \boldsymbol{B}_0^2)\,\mathrm{d}V$ and $W_{\mathrm{f2}} = (1/2\mu_0)\int \boldsymbol{B}^2\,\mathrm{d}V - (1/2\mu_0)\int \boldsymbol{B}_0^2\,\mathrm{d}V$.

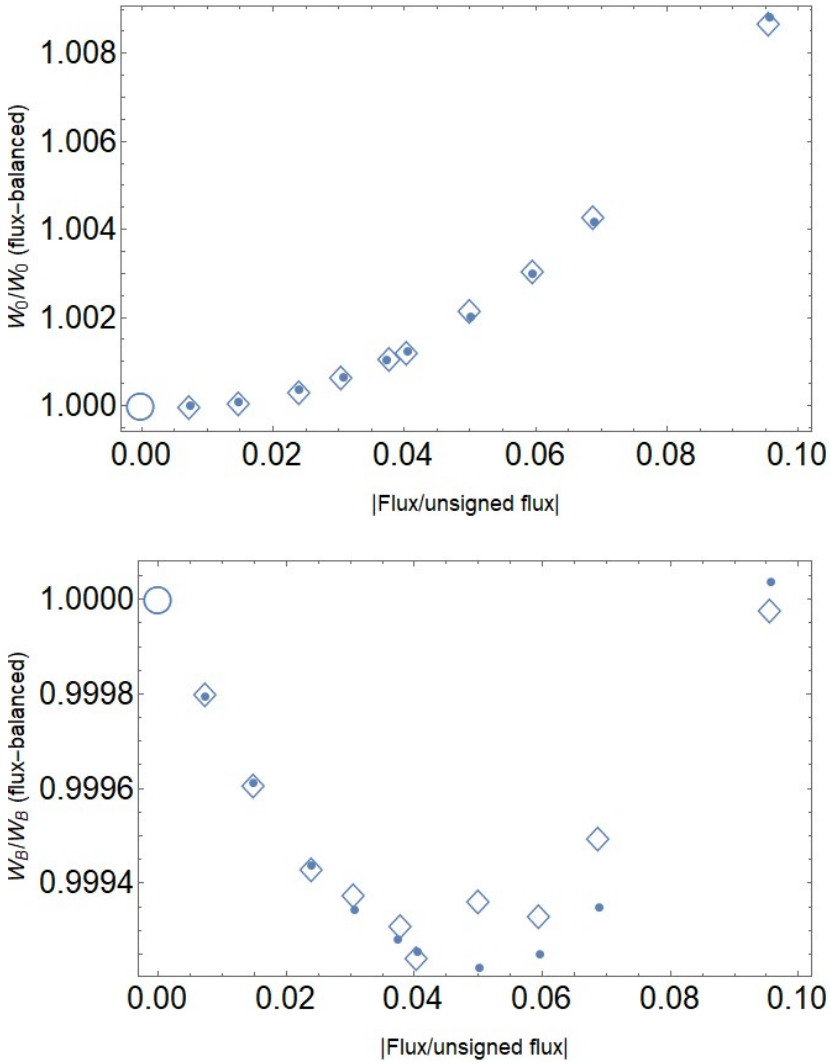

Figure 5. The energy of the potential field W_0 and that of the total field W_B as functions of the ratio of flux to unsigned flux for a bipole test case. The vertical axes are normalised to the values of the quantities for the flux-balanced case (the empty circle). The filled circles are the uniform background case, and the diamonds are the random background case.

Different results for these two values indicate departure from the divergence-free condition in the volume. It must be noted, however, that $W_{\rm f1} = W_{\rm f2}$ is a necessary but not sufficient condition for a divergence-free field. One can have $W_{\rm f1} = W_{\rm f2}$ but $\nabla \cdot \boldsymbol{B} \neq 0$. A necessary and sufficient condition for a divergence-free field is provided by the Helmholtz decomposition.

Our analysis shows that care must be taken when calculating and stating the "free energy" of a model field, as the two ways of calculating free energy, $W_{\rm f1}$ and $W_{\rm f2}$, can give different answers.

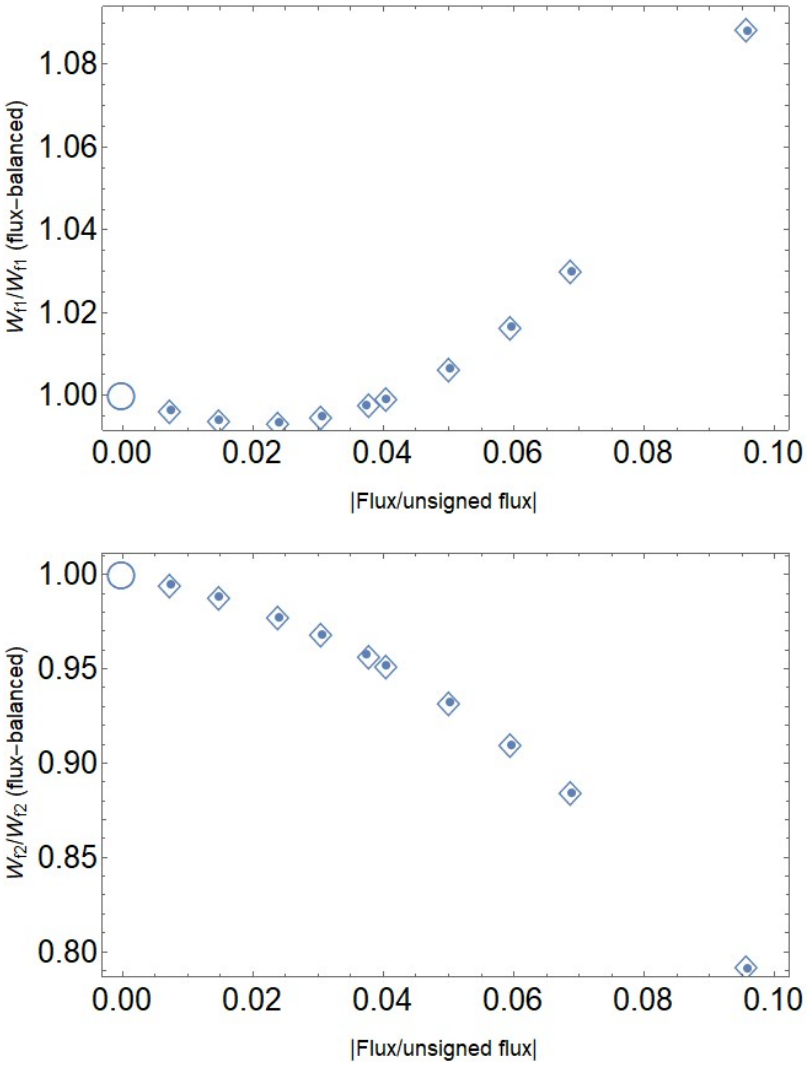

Figure 6. The energies W_{f1} and W_{f2} as functions of the ratio of flux to unsigned flux for a bipole test case. The vertical axes are normalised to the values of the quantities for the flux-balanced case (the empty circle). The filled circles are the uniform background case, and the diamonds are the random background case.

The test presented here can, in principle, be applied to any model field $\boldsymbol{B}$ in a regular volume. For example, it can be applied to the results of magnetohydrodynamics codes. The test requires only the normal components of $\boldsymbol{B}$ at the boundaries, used to construct $\boldsymbol{B}_0$, after which the calculations and comparisons of energies readily follow.

Acknowledgments This work was funded in part by an Australian Research Council Discovery Project (DP160102932). The authors thank Don Melrose and the reviewer for helpful comments.

Disclosure of Potential Conflicts of Interest The authors declare that they have no conflicts of interest.

Appendix

In this appendix we describe the Checkerboard Relaxation Method Used for Potential field reconstruction code (CRUMP) and its application to a simple test case. We show that the numerical error for this case is consistent with the truncation error of the second-order scheme employed by the code.

A. Details of the CRUMP Code

The CRUMP code solves the scalar Laplace equation in a Cartesian box using a second-order finite difference method. Specifically, second-order centered differences are used to approximate the Laplacian at interior points (Press *et al.*, 1992). At the boundary, ghost points are used to enforce Neumann boundary conditions to second order. The code is implemented in the Fortran2003 language (Metcalf, Reid, and Cohen, 2011) and is parallelized for shared-memory parallel computers using the OpenMP standard (Chandra *et al.*, 2001).

The discrete system is solved using the checkerboard (red-black) Gauss-Sidel relaxation method (Press *et al.*, 1992; Briggs, Henson, and McCormick, 2000). Successive over-relaxation with Chebyshev acceleration is used to speed up convergence of the scheme (Press *et al.*, 1992). In principle, to achieve convergence for a mesh with N mesh points in each dimension, over-relaxation takes of order N iterations to converge (Press *et al.*, 1992). It is difficult to compute the exact number required *a priori*, so in practice, the calculation is halted when the difference between successive iterations is below a user-defined threshold. The code computes the scalar potential, and the magnetic field is found numerically using the second-order centered difference approximation to the gradient.

Since the code uses Neumann boundary conditions on all six boundaries of the Cartesian domain, there is no unique solution to the linear system: a constant can be added to any solution to produce another one that both solves Laplace's equation and satisfies the boundary conditions (Briggs, Henson, and McCormick, 2000). To break this degeneracy, we pick the particular solution whose mean over the domain is zero. This condition is enforced at each iteration by making the replacement

$$u \to u - \langle u \rangle, \tag{21}$$

where $\langle u \rangle$ is the mean of u over all mesh points.

B. Numerical Error Scaling for the CRUMP Code

To demonstrate the accuracy of the code we apply it to a simple analytic test case and measure the numerical error for different mesh resolutions. We show that the code achieves the expected second-order accuracy.

We measure the numerical error using two metrics. The first metric is the component-wise maximum difference between the numerical and analytic solutions, *i.e.*

$$E_{\text{diff}} = \max\left(\boldsymbol{B} - \boldsymbol{B}_{\text{ex}}\right), \tag{22}$$

where $\boldsymbol{B}_{\text{ex}}$ is the exact analytic field. The second metric is the maximum value of the divergence over the domain, *i.e.*

$$E_{\text{div}}(\boldsymbol{B}) = \max\left(\nabla \cdot \boldsymbol{B}\right). \tag{23}$$

The divergence is computed numerically using a second-order centered difference scheme. As a result, additional truncation error is introduced by this approximation. To measure this error, it is instructive to compute E_{div} for the the exact solution too.

To test CRUMP, we apply it to the simple analytic magnetic field with components

$$B_x = -\frac{k}{A}\sin\left(kx\right)\cos\left(ky\right)\cosh[l(z - L_z)], \tag{24}$$

$$B_y = -\frac{k}{A}\cos\left(kx\right)\sin\left(ky\right)\cosh[l(z - L_z)], \tag{25}$$

and

$$B_z = +\frac{l}{A}\cos\left(kx\right)\cos\left(ky\right)\sinh[l(z - L_z)]. \tag{26}$$

We set $A = \sinh(l)l$, $k = 2\pi$, and $L_z = 1$. The variable l must take the value $l = \sqrt{2}k$ to ensure that $\nabla \cdot \boldsymbol{B} = 0$.

We construct Neumann boundary conditions for CRUMP from Equations 24–26. We compute the solution in a domain that has a length of unity in each dimension and the same number of mesh points in each dimension. We perform tests at different resolutions by increasing the number of mesh points.

Figure 7 shows the values of the metrics defined by Equations 22 and 23 computed from the numerical solutions produced by CRUMP for different values of the mesh spacing h. For each test, we terminate the relaxation when the difference between iterations is below 10^{-15}, which is close to the double-precision machine epsilon.

Figure 7 also shows the value of the metric E_{div} computed for the analytic solution. For all resolutions, the value of E_{div} for the numerical solution is smaller than that obtained by applying the second-order centered difference scheme directly on the analytic solution, implying that we achieve a small error in the actual divergence for this particular test case.

Figure 7 shows power-law fits to each of the data sets (straight lines). We find that the power-law indices are close to a value of two. This indicates that the numerical error for CRUMP is consistent with the truncation error of the second-order difference scheme used.

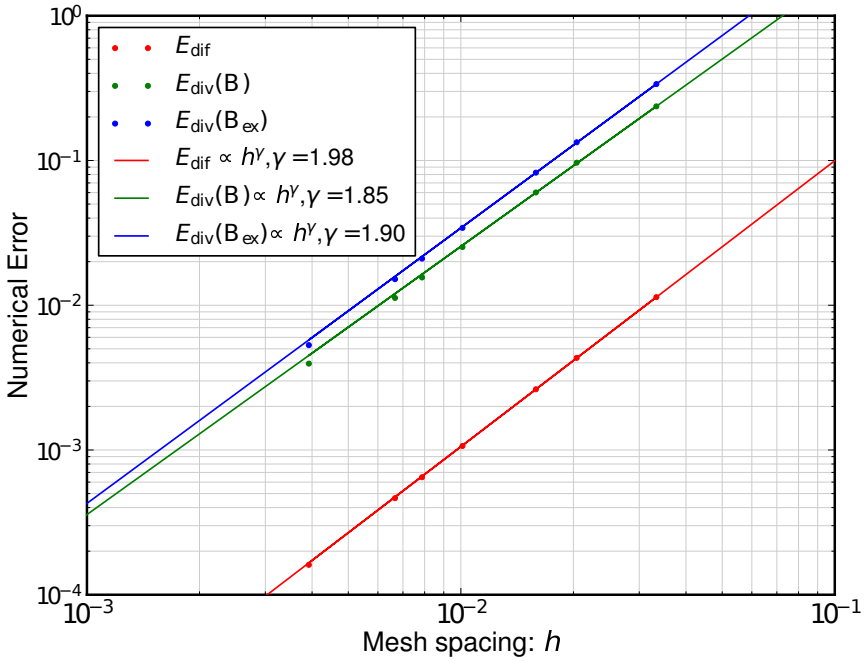

Figure 7. Numerical error metrics for the CRUMP code at different resolutions. The metrics measure the maximum difference between the numerical and analytic solutions ($E_{\rm diff}$) and the maximum value of the divergence ($E_{\rm div}(\boldsymbol{B})$). The data set $E_{\rm div}(\boldsymbol{B}_{\rm ex})$ shows the divergence metric computed for the analytic magnetic field. Because the evaluation of this metric involves numerically derivatives, its value is non-zero even for the exact solution. The straight lines show power-law fits to the data. The power-law indices are close to two in each case, indicating the code achieves second-order scaling, as expected for a second-order scheme.

References

Alissandrakis, C.E.: 1981, On the computation of constant alpha force-free magnetic field. *Astron. Astrophys.* **100**, 197. ADS.

Amari, T., Boulmezaoud, T.Z., Aly, J.J.: 2006, Well posed reconstruction of the solar coronal magnetic field. *Astron. Astrophys.* **446**, 691. DOI. ADS.

Barnes, G., Leka, K.D., Schrijver, C.J., Colak, T., Qahwaji, R., Ashamari, O.W., Yuan, Y., Zhang, J., McAteer, R.T.J., Bloomfield, D.S., Higgins, P.A., Gallagher, P.T., Falconer, D.A., Georgoulis, M.K., Wheatland, M.S., Balch, C., Dunn, T., Wagner, E.L.: 2016, A Comparison of Flare Forecasting Methods. I. Results from the "All-Clear" Workshop. *Astrophys. J.* **829**, 89. DOI. ADS.

Briggs, W.L., Henson, V.E., McCormick, S.F.: 2000, *A multigrid tutorial (2nd ed.)*, Society for Industrial and Applied Mathematics, Philadelphia, PA, USA. ISBN 0-89871-462-1. DOI.

Chandra, R., Dagum, L., Kohr, D., Maydan, D., McDonald, J., Menon, R.: 2001, *Parallel programming in openmp*, Morgan Kaufmann Publishers Inc., San Francisco, CA, USA. ISBN 1-55860-671-8, 9781558606715.

Chiu, Y.T., Hilton, H.H.: 1977, Exact Green's function method of solar force-free magnetic-field computations with constant alpha. I - Theory and basic test cases. *Astrophys. J.* **212**, 873. DOI. ADS.

DeRosa, M.L., Wheatland, M.S., Leka, K.D., Barnes, G., Amari, T., Canou, A., Gilchrist, S.A., Thalmann, J.K., Valori, G., Wiegelmann, T., Schrijver, C.J., Malanushenko, A., Sun, X., Régnier, S.: 2015, The Influence of Spatial resolution on Nonlinear Force-free Modeling. *Astrophys. J.* **811**, 107. DOI. ADS.

Metcalf, M., Reid, J., Cohen, M.: 2011, *Modern fortran explained*, 4th edn. Oxford University Press, Inc., New York, NY, USA. ISBN 0199601410, 9780199601417.

Moraitis, K., Tziotziou, K., Georgoulis, M.K., Archontis, V.: 2014, Validation and Benchmarking of a Practical Free Magnetic Energy and Relative Magnetic Helicity Budget Calculation in Solar Magnetic Structures. *Solar Phys.* **289**, 4453. DOI. ADS.

Moraitis, K., Toutountzi, A., Isliker, H., Georgoulis, M., Vlahos, L., Chintzoglou, G.: 2016, An observationally-driven kinetic approach to coronal heating. *Astron. Astrophys.* **596**, A56. DOI. ADS.

Press, W.H., Teukolsky, S.A., Vetterling, W.T., Flannery, B.P.: 1992, *Numerical Recipes in FORTRAN. The Art of Scientific Computing*. ADS.

Su, J.T., Jing, J., Wang, S., Wiegelmann, T., Wang, H.M.: 2014, Statistical Study of Free Magnetic Energy and Flare Productivity of Solar Active Regions. *Astrophys. J.* **788**, 150. DOI. ADS.

Valori, G., Kliem, B., Fuhrmann, M.: 2007, Magnetofrictional Extrapolations of Low and Lou's Force-Free Equilibria. *Solar Phys.* **245**, 263. DOI. ADS.

Valori, G., Kliem, B., Török, T., Titov, V.S.: 2010, Testing magnetofrictional extrapolation with the Titov-Démoulin model of solar active regions. *Astron. Astrophys.* **519**, A44. DOI. ADS.

Valori, G., Démoulin, P., Pariat, E., Masson, S.: 2013, Accuracy of magnetic energy computations. *Astron. Astrophys.* **553**, A38. DOI. ADS.

Wheatland, M.S.: 2007, Calculating and Testing Nonlinear Force-Free Fields. *Solar Phys.* **245**, 251. DOI. ADS.

Wheatland, M.S., Sturrock, P.A., Roumeliotis, G.: 2000, An Optimization Approach to Reconstructing Force-free Fields. *Astrophys. J.* **540**, 1150. DOI. ADS.

Wiegelmann, T., Inhester, B.: 2010, How to deal with measurement errors and lacking data in nonlinear force-free coronal magnetic field modelling? *Astron. Astrophys.* **516**, A107. DOI. ADS.

Wiegelmann, T., Thalmann, J.K., Inhester, B., Tadesse, T., Sun, X., Hoeksema, J.T.: 2012, How Should One Optimize Nonlinear Force-Free Coronal Magnetic Field Extrapolations from SDO/HMI Vector Magnetograms? *Solar Phys.* **281**, 37. DOI. ADS.